Planetary and Space Science 58 (2010) 2044–2049

Contents lists available at ScienceDirect

Planetary and Space Science

journal homepage: www.elsevier.com/locate/pss

Trajectory and atmospheric structure from entry probes: Demonstration of a real-time reconstruction technique using a simple direct-to-Earth radio link

Paul Withers *

Center for Space Physics, Boston University, 725 Commonwealth Avenue, Boston, MA 02215, USA

ARTICLE INFO

Article history:
Received 19 May 2010
Received in revised form
12 October 2010
Accepted 15 October 2010
Available online 23 October 2010

Keywords:
Mars
Atmospheric entry
Accelerometer
Radio science

ABSTRACT

The reconstruction of the trajectory and atmospheric structure associated with an entry probe has traditionally relied upon onboard accelerometer measurements. Here we outline an equivalent reconstruction technique that uses Doppler-shifted direct-to-Earth transmissions instead. A critical assumption is that the entry probe's angle of attack is zero. The technique is successfully demonstrated on the atmospheric entry of the Mars Exploration Rover Opportunity, terminating at parachute deployment. This technique can be applied in real-time, which supports mission operations and public engagement. It can also be applied to entry probes that fail during their high-risk atmospheric entry.

1. Introduction

Many entry probes maintain a radio link to a receiver whose trajectory is known and that is capable of recording the frequency of the received signals. This receiver can be on Earth, in orbit around the planetary object that is the target of the entry probe, or flying past this planetary object. The trajectory of an entry probe is traditionally reconstructed from integration of onboard accelerometer measurements (Withers and Smith, 2006, and references therein). Once the trajectory is obtained, the atmospheric density, pressure, and temperature along the trajectory can be reconstructed as well (Withers and Smith, 2006, and references therein). Successful reconstruction requires that the accelerometer data is returned to Earth for analysis. However, the necessary data transmission may not occur until some time after atmospheric entry. In the worst case scenario of a mission that fails during atmospheric entry, the onboard accelerometer data will be irrevocably lost. In this paper, we use the Mars Exploration Rover Opportunity as a case study to investigate whether trajectory and atmospheric structure associated with an entry probe can be reconstructed from time series of received radio frequencies. Our aim is limited to determining whether or not this concept is viable, thus postponing the development of the concept to a level suitable for immediate operational use to future work.

We have identified several reasons why this concept is worthy of investigation. A near-real time trajectory reconstruction provides a rapid estimate of landing site location, which is useful for a range of engineering purposes. It is also useful for the identification of any anomalous events that may have occurred during entry. A near-real-time atmospheric structure reconstruction provides a rapid assessment of the accuracy of predicted environmental conditions, which is useful for a range of engineering purposes. It also offers a tangible data product for engaging the public. Public interest in the atmospheric entry phase of missions is intense, yet few results are available until hours or days after entry. If a mission fails during atmospheric entry (e.g. Beagle 2, Mars Polar Lander), then this technique may be able to provide the mission's only scientific results.

Section 2 introduces the main concept of this work. Section 3 outlines how this concept was applied to the atmospheric entry of Opportunity. Section 4 reports the reconstructed trajectory and atmospheric structure obtained for Opportunity. Section 5 discusses the implications of this work.

2. Concept

Our objective is to relate the line-of-sight velocity, which can be found from the Doppler shift in the radio signal, to the vector aerodynamic acceleration. In principle, accomplishment of this objective suggests that accelerometer measurements of the aerodynamic acceleration are no longer needed for trajectory and atmospheric structure reconstruction. However, the established accuracy of reconstructions using accelerometer measurements means that the technique introduced here should be regarded as complementary to accelerometer-based techniques. The velocity vector of the entry probe at time t_0, $\underline{v_0}$, is related to the velocity

* Tel.: +1 617 353 1531; fax: +1 617 353 6463.
E-mail address: withers@bu.edu

0032-0633/$ - see front matter © 2010 Elsevier Ltd. All rights reserved.
doi:10.1016/j.pss.2010.10.005

vector at time $t_1 = t_0 + \Delta t$, $\underline{v}_1$, via the acceleration vector, $\underline{a}$:

$$\underline{v}_1 = \underline{v}_0 + \underline{a}\Delta t \tag{1}$$

This is valid in an inertial frame, which we label as the "active frame". Careful consideration of reference frames is important for trajectory reconstruction. The acceleration vector, $\underline{a}$, is the sum of the gravitational acceleration, $\underline{g}$, and the aerodynamic acceleration, $\underline{a}_{aero}$:

$$\underline{a} = \underline{g} + \underline{a}_{aero} \tag{2}$$

If $\underline{l}_0$ is the unit vector along the line-of-sight from the entry probe to the receiver, then Eqs. (1) and (2) can be rearranged to yield

$$\underline{a}_{aero} \cdot \underline{l}_0 = \frac{1}{\Delta t}(\underline{v}_1 \cdot \underline{l}_0 - \underline{v}_0 \cdot \underline{l}_0) - \underline{g} \cdot \underline{l}_0 \tag{3}$$

A trajectory reconstruction requires $\underline{a}_{aero}$, not merely one component of $\underline{a}_{aero}$. Fortunately, the design of typical entry probes offers a solution. Entry vehicles are often designed to have minimal lift and fly at close to zero angle of attack. In the lift-less limit

$$\underline{a}_{aero} = -k(\underline{v}_0 - \underline{v}_{atm}) \tag{4}$$

where $\underline{v}_{atm}$ is the velocity of the planetary atmosphere in the active frame and k is an unknown constant of proportionality. Thus

$$\underline{a}_{aero} \cdot \underline{l}_0 = -k(\underline{v}_0 \cdot \underline{l}_0 - \underline{v}_{atm} \cdot \underline{l}_0) \tag{5}$$

Rearranging Eqs. (3) and (5) to solve for k, we have

$$k = \frac{-[\frac{1}{\Delta t}(\underline{v}_1 \cdot \underline{l}_0 - \underline{v}_0 \cdot \underline{l}_0) - \underline{g} \cdot \underline{l}_0]}{(\underline{v}_0 \cdot \underline{l}_0 - \underline{v}_{atm} \cdot \underline{l}_0)} \tag{6}$$

This expression for k can be substituted into Eq. (4) to obtain

$$\underline{a}_{aero} = \frac{(\underline{v}_0 - \underline{v}_{atm})}{(\underline{v}_0 \cdot \underline{l}_0 - \underline{v}_{atm} \cdot \underline{l}_0)} \left[\frac{1}{\Delta t}(\underline{v}_1 \cdot \underline{l}_0 - \underline{v}_0 \cdot \underline{l}_0) - \underline{g} \cdot \underline{l}_0 \right] \tag{7}$$

We only apply this expression to the entry phase of atmospheric flight, not any subsequent descent phases using parachutes. Entry probe dynamics increase in complexity after parachute deployment (e.g. Dzierma et al., 2007; Kazeminejad et al., 2007; Karkoschka et al., 2007; Lorenz et al., 2007). The atmospheric motion, $\underline{v}_{atm}$, can be approximated using a model of the planet's winds. For some planets, such as Mars, solid body rotation at the rotation rate of the planet can be assumed. For super-rotating objects, such as Venus and Titan, another model should be used.

The main quantity that must be provided by measurement in order for Eq. (7) to provide $\underline{a}_{aero}$ is $\underline{v} \cdot \underline{l}$. Using the classical Doppler shift, $\underline{v} \cdot \underline{l}$ satisfies

$$\underline{v} \cdot \underline{l} = -c\frac{(f_R - f_T)}{f_T} \tag{8}$$

where c is the speed of light, f_R is the received frequency, f_T is the transmitted frequency, and the direction of $\underline{l}$ is such that $\underline{v} \cdot \underline{l}$ is positive for increasing transmitter–receiver separation. Hence a time series of $\underline{v} \cdot \underline{l}$ can be obtained from knowledge of f_T and a time series of f_R. Matters are simplest if f_T is constant during atmospheric entry, although environmental effects such as heating and acceleration can change f_T (e.g. Atkinson et al., 1998). Given f_R and f_T, the value of $\underline{v} \cdot \underline{l}$ can be found using Eq. (8) and knowledge of the trajectories of the receiver and transmitter at the appropriate time.

Thus we obtain the following series of equations, in which $\underline{x}$ is position

$$\underline{x}_{i+1} = \underline{x}_i + \underline{v}_i \Delta t \tag{9}$$

$$\underline{v}_{i+1} = \underline{v}_i + \underline{a}_i \Delta t \tag{10}$$

$$\underline{a}_{i+1} = \frac{(\underline{v}_i - \underline{v}_{atm,i})}{(\underline{v}_i \cdot \underline{l}_i - \underline{v}_{atm,i} \cdot \underline{l}_i)} \left[\frac{1}{\Delta t}(\underline{v}_{i+1} \cdot \underline{l}_i - \underline{v}_i \cdot \underline{l}_i) - \underline{g} \cdot \underline{l}_i \right] \tag{11}$$

With the minor assumption that $\underline{v}_{i+1} \cdot \underline{l}_i$, which is not measured, equals $\underline{v}_{i+1} \cdot \underline{l}_{i+1}$, which is measured, all quantities on the right-hand side of Eq. (11) are known. Thus Eqs. (9)–(11) can be integrated forwards in time given suitable initial conditions. Initial conditions for $\underline{x}$ and $\underline{v}$ can be found from trajectory analysis prior to atmospheric entry and an initial condition for $\underline{a}$ is simply $\underline{a} = \underline{g}$.

3. Application to the atmospheric entry of Opportunity

The received frequency recorded as a function of time at a NASA Deep Space Network (DSN) station during Opportunity's atmospheric entry has been reported by Johnston et al. (2004) (their Fig. 6) and is reproduced in Fig. 1. However, the scale on the time axis in the original figure suggests that the figure spans 200 s. This is much too short. For example, the duration of appreciable aerodynamic deceleration should be over 100 s and the interval between parachute deployment and first ground contact should be approximately 100 s (Johnston et al., 2004; Withers and Smith, 2006; Withers and Murphy, 2009). We used the stated times of parachute deployment and rocket firing, events which are visible in Figure 6 of Johnston et al. (2004) and highlighted in Fig. 1 of this work, to obtain a revised time scale which is shown in Fig. 1 of this work. Tickmarks now correspond to intervals of 100 s. Frequency and time values were extracted from the figure using the DataThief tool (www.datathief.org).

JPL's SPICE tools were used extensively in this work. SPICE is a powerful framework for representing the positions, motions, and orientations of spacecraft and planets. Additional descriptions of the capabilities of SPICE can be found at http://naif.jpl.nasa.gov/naif/. Although the available documentation is extensive, the best way to learn SPICE is to use SPICE. Received times at Earth were adjusted to transmitted times at Mars by using SPICE to calculate the light time between Earth and Mars. The transmitted frequency, which is necessary to infer entry probe speed from received frequency, is not stated by Johnston et al. (2004). However, it can be inferred from the received frequency corresponding to transmissions prior to atmospheric entry. The position and velocity vectors of Opportunity prior to atmospheric entry were obtained from SPICE kernel

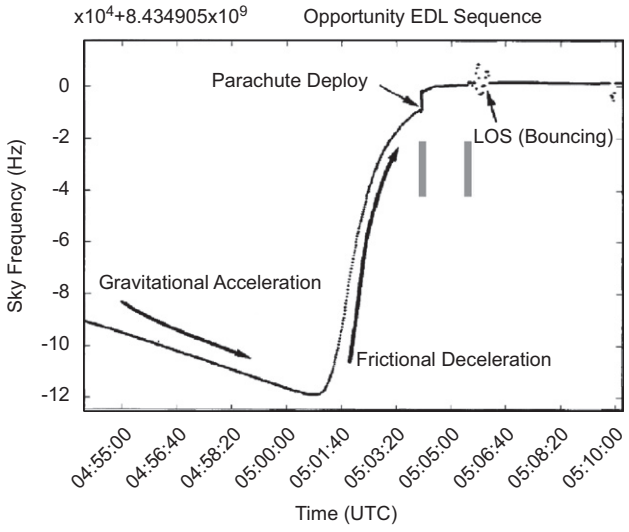

Fig. 1. Received frequency as a function of time for Opportunity. Modified from Fig. 6 of Johnston et al. (2004). Sky frequencies indicated on the vertical axis are transformed into actual received frequencies by multiplying 10^4 and adding 8.434905 GHz. The times indicated on the horizontal axis differ from those in Johnston et al. (2004), which are incorrect. The left vertical grey bar highlights parachute deployment at 05:04:08 UTC, which is easy to see, and the right vertical grey bar highlights rocket firing at 05:05:31 UTC, which is harder to see. The tickmarks on the horizontal axis corresponds to intervals of 100 s.

spk_b_c_030708-040125_recon.bsp for the desired times using standard SPICE tools. The trajectory of the receiver depends on which DSN station recorded the data reported by Johnston et al. (2004). The speed of Earth relative to Opportunity at entry is about 19.30 km s^{-1}. Using different DSN locations alters this value by 0.15 km s^{-1} or less than 1%, which is not very large for the accuracies desired in this work, so a receiver location at Earth's centre of mass was assumed. SPICE tools were used to find the state vectors (position and velocity) of Opportunity and the receiver in an inertial frame at the desired times, from which the line-of-sight speed of Opportunity relative to the receiver was determined. Calculation of the Doppler shift associated with this speed showed that the transmitted frequency was 8.4353524 GHz. This frequency was assumed to remain constant throughout entry. Note that the frequency of 8.434905 GHz indicated in Fig. 1 corresponds to Opportunity at rest on the surface of Mars, when the transmitter is moving relative to the receiver at several km s^{-1} due to the motions of Earth and Mars. Hence 8.434905 GHz is not the transmitted frequency. The unit vectors introduced in Section 2 were found from the calculated position vectors of Opportunity and the receiver.

The time series of received frequencies were then processed to give a series of line-of-sight speeds of Opportunity relative to the receiver as a function of transmission time at Mars. The integration of Eqs. (9)–(11) was performed in a Mars-fixed reference frame. Accordingly, the line-of-sight speed of the centre of mass of Mars relative to the receiver was subtracted from the line-of-sight speed of Opportunity relative to the receiver to give the line-of-sight speed of Opportunity relative to the centre of mass of Mars.

The UTC start time for the trajectory reconstruction was 2004 JAN 25 04:48:41.711, corresponding to a radial distance from Mars of 3522.2 km. This was the distance defined by the Mars Exploration Rover project as the atmospheric entry interface (Kass et al., 2004). The initial position and velocity of Opportunity in a Mars-fixed reference frame were obtained using SPICE tools and the initial aerodynamic acceleration was set to zero. The gravitational acceleration was calculated using an inverse-square law with $GM = 4.2828 \times 10^4$ km^3 s^{-2} (Lodders and Fegley, 1998). The trajectory reconstruction was terminated at parachute deployment.

4. Results

A reconstruction of the trajectory and atmospheric structure associated with Opportunity has already been performed using onboard accelerometer data. Scientific results are reported in Withers and Smith (2006) and the data products are archived in Withers and Murphy (2009).

Fig. 2 shows the magnitude of the reconstructed aerodynamic acceleration as a function of time, and includes comparisons to the results of Withers and Murphy (2009). The inferred values of aerodynamic acceleration are reasonable for approximately 200 s preceding parachute deployment. The peak deceleration found in this work, 62.5 m s^{-2}, is within 2% of the value reported by Withers and Murphy (2009), 61.5 m s^{-2}.

Figs. 3 and 4 show the reconstructed atmosphere-relative speed and altitude as functions of time, and include comparisons to the results of Withers and Murphy (2009). All altitudes used in this work are radial distances above the landing site at 3394.1 km. The speed at parachute deployment found in this work, 596 m s^{-1}, is over 35% greater than the value reported by Withers and Murphy (2009), 430 m s^{-1}, but this difference of 166 m s^{-1} is only 3% of the atmosphere-relative speed at entry of 5.5 km s^{-1}. The altitude at parachute deployment found in this work, 5.0 km, is less than the value reported by Withers and Murphy (2009), 6.2 km, but this difference is only 1% of the vertical distance between atmospheric entry and parachute deployment.

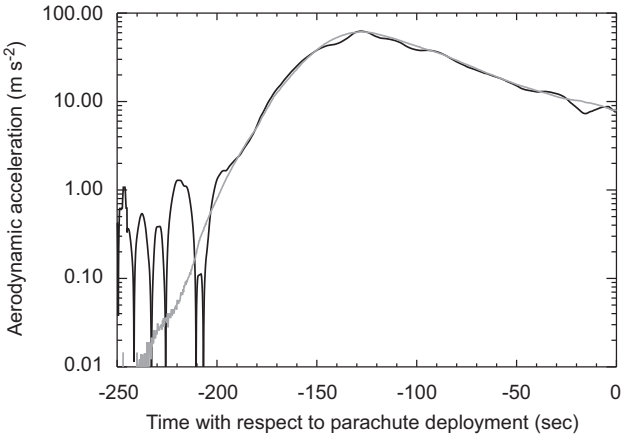

Fig. 2. Aerodynamic acceleration determined in this work (black line) and from Withers and Murphy (2009) (grey line) as functions of time.

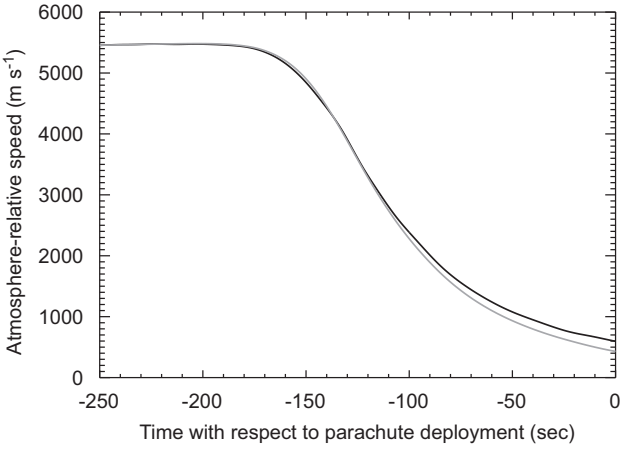

Fig. 3. Atmosphere-relative speed ($|\underline{v_0} - \underline{v_{atm}}|$) determined in this work (black line) and from Withers and Murphy (2009) (grey line) as functions of time. Relative to the centre of mass of Mars, the magnitude of $\underline{v_{atm}}$ is two hundred metres per second.

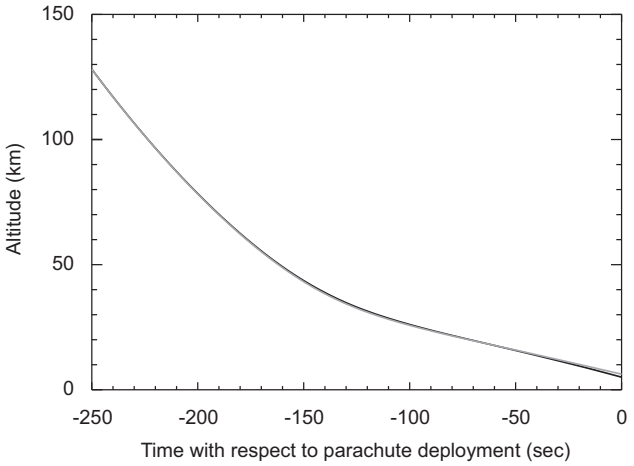

Fig. 4. Altitude determined in this work (black line) and from Withers and Murphy (2009) (grey line) as functions of time.

Fig. 5 shows the individual components of the reconstructed atmosphere-relative velocity. Opportunity's motion is predominantly

eastward and the vertical descent speed is on the order of 500–1000 m s^{-1}. Figs. 6–8 show the reconstructed atmosphere-relative speed, latitude, and longitude, respectively, as functions of altitude, and include comparisons to the results of Withers and Murphy (2009). Differences in speed are only apparent below 20 km. Differences in latitude and longitude are minor. The differences in latitude and longitude at parachute deployment are 0.01° and 0.3°, respectively. Again, differences in longitude are only apparent below 20 km.

Since the reconstructed aerodynamic acceleration is unreliable at high altitudes, the atmospheric structure reconstruction commenced at 80 km altitude. This used the traditional approach adopted by many previous workers (Withers and Smith, 2006, and references therein). Atmospheric density, ρ, is related to the magnitude of the aerodynamic acceleration (Magalhães et al., 1999):

$$m|a_{aero}| = \frac{\rho A(\underline{v}-\underline{v}_{atm})^2 C}{2} \quad (12)$$

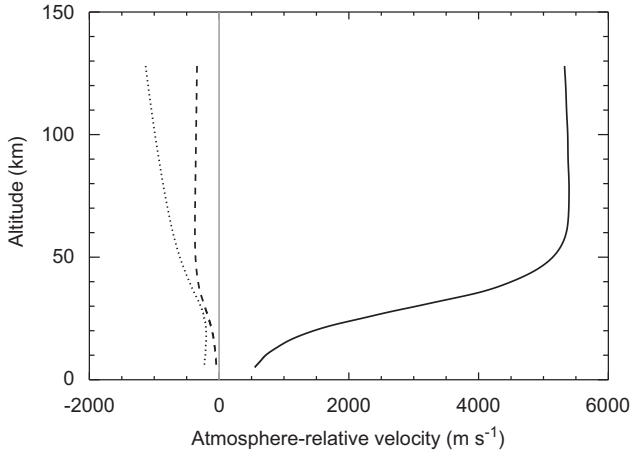

Fig. 5. Components of the atmosphere-relative velocity, $\underline{v}_0-\underline{v}_{atm}$. The solid line is the zonal component, positive eastward. The dotted line is the radial component, positive upwards. The dashed line is the meridional component, positive southwards. The vertical grey line indicates zero velocity.

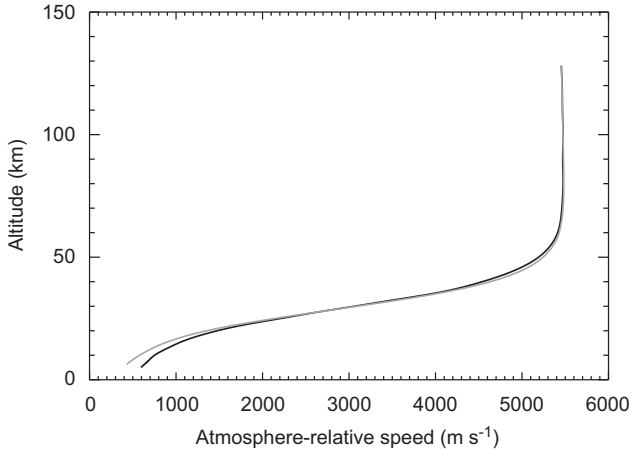

Fig. 6. Atmosphere-relative speed ($|\underline{v}_0-\underline{v}_{atm}|$) determined in this work (black line) and from Withers and Murphy (2009) (grey line) as functions of altitude. Relative to the centre of mass of Mars, the magnitude of $\underline{v}_{atm}$ is two hundred metres per second.

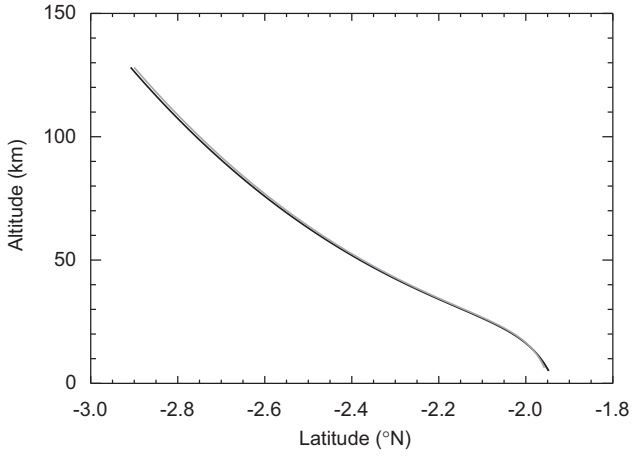

Fig. 7. Latitude determined in this work (black line) and from Withers and Murphy (2009) (grey line) as functions of altitude.

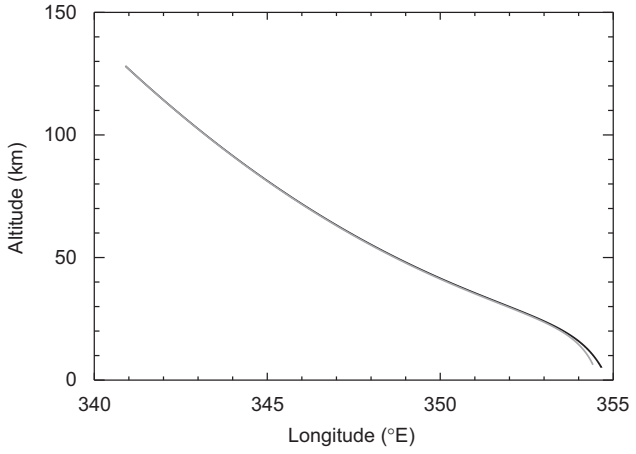

Fig. 8. Longitude determined in this work (black line) and from Withers and Murphy (2009) (grey line) as functions of altitude.

where m is the spacecraft mass (832.2 kg—Desai and Knocke, 2004), A is the reference area of the spacecraft (disk of diameter 2.648 m—Schoenenberger et al., 2005), and C is an aerodynamic coefficient, which is usually on the order of 2 (Withers et al., 2003). The aerodynamic coefficients needed to relate density to aerodynamic acceleration were obtained from the aerodynamic database published by Schoenenberger et al. (2005) assuming that the angle of attack was always zero. Atmospheric pressure, p, is related to ρ by the equation of hydrostatic equilibrium:

$$\frac{dp}{dr} = -\rho g \quad (13)$$

where g is the magnitude of the gravitational acceleration introduced in Section 3 and r is distance from the centre of mass. Atmospheric temperature, T, is related to ρ and p by the ideal gas law:

$$\mu p = \rho \frac{R}{N_A} T \quad (14)$$

where $\mu = 43.49$ g mol^{-1} is the mass of one mole of the martian atmosphere, R is the universal gas constant, and N_A is Avogrado's number (Magalhães et al., 1999). A temperature of 120 K was assumed at the upper boundary to provide a boundary condition for the equation of hydrostatic equilibrium. The Knudsen (Kn) and

Mach (Ma) numbers were also calculated. Kn is defined as

$$\mathrm{Kn} = \frac{1}{\sqrt{2}\pi d^2 n D} \tag{15}$$

where d is the diameter of an atmospheric molecule (4.64×10^{-10} m—Schoenenberger et al., 2005), n, which satisfies $n = N_A\rho/\mu$, is the atmospheric number density, and D is the diameter of the entry probe. Ma is defined as

$$\mathrm{Ma} = \frac{|\underline{v} - \underline{v}_{\mathrm{atm}}|}{(\gamma p/\rho)^{1/2}} \tag{16}$$

where γ is the ratio of the heat capacity at constant pressure to the heat capacity at constant volume of the martian atmosphere (7/5 for an ideal linear polyatomic gas like CO_2—Atkins, 2002). Reconstructed density, pressure, temperature, Kn, and Ma are shown in Figs. 9–13 as functions of altitude and compared to the results of Withers and Murphy (2009). Results in Figs. 9–13 have been smoothed to reduce high frequency oscillations. The plotted value at a particular altitude is the mean (arithmetic mean for temperature and Ma, geometric mean for density, pressure, and Kn) of all results within ± 5 km of that altitude.

Density differences are $<20\%$ between 20 and 70 km. Pressure differences are $<20\%$ between 15 and 70 km. Temperature

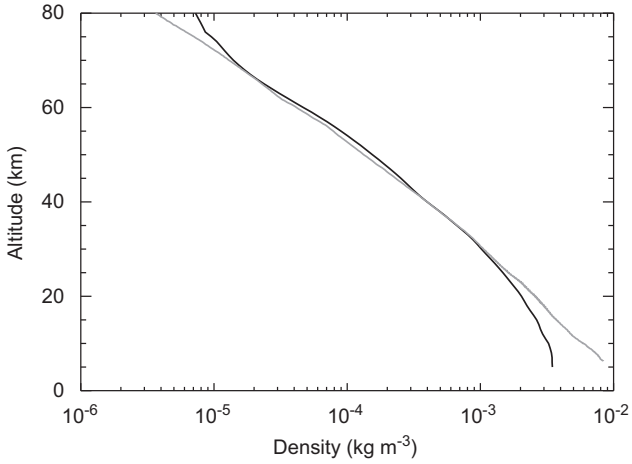

Fig. 9. Density determined in this work (black line) and from Withers and Murphy (2009) (grey line) as functions of altitude.

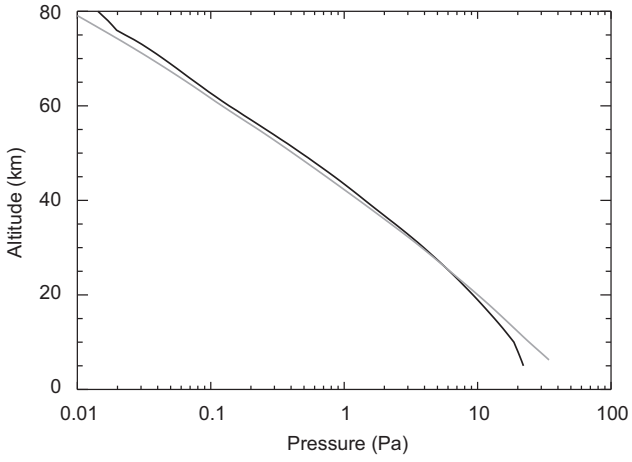

Fig. 10. Pressure determined in this work (black line) and from Withers and Murphy (2009) (grey line) as functions of altitude.

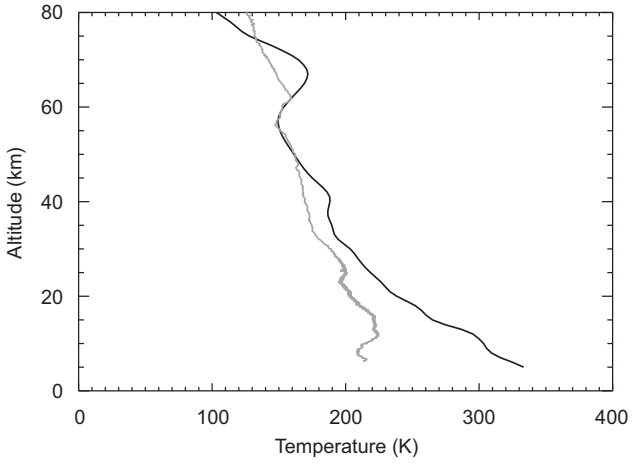

Fig. 11. Temperature determined in this work (black line) and from Withers and Murphy (2009) (grey line) as functions of altitude.

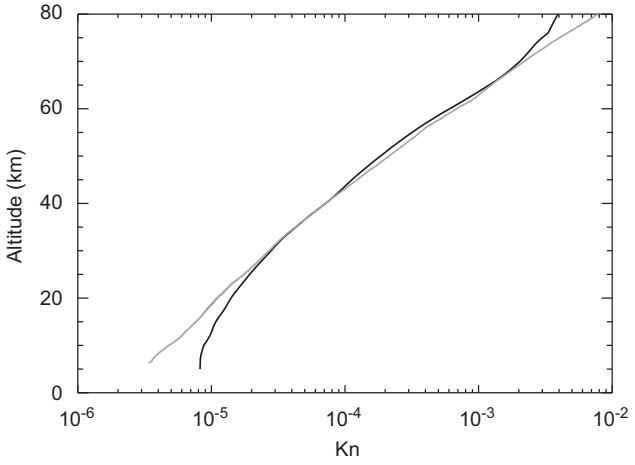

Fig. 12. Knudsen number (Kn) determined in this work (black line) and from Withers and Murphy (2009) (grey line) as functions of altitude.

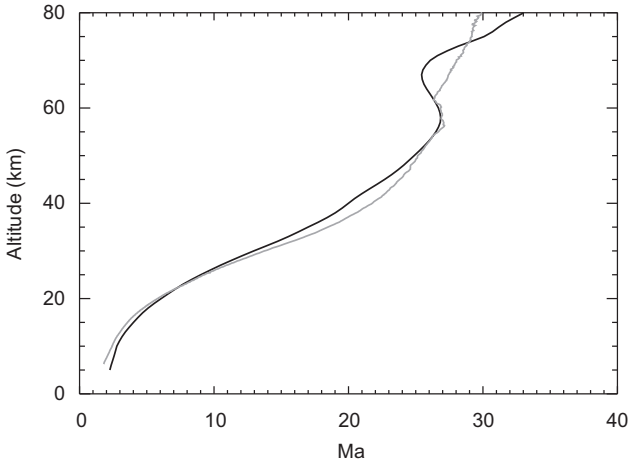

Fig. 13. Mach number (Ma) determined in this work (black line) and from Withers and Murphy (2009) (grey line) as functions of altitude.

differences are <30 K between 20 and 80 km, although they exceed 100 K close to parachute deployment. Knudsen differences are $<20\%$ between 20 and 70 km, although they exceed 50% below 15 km. Mach differences are $<20\%$ at all altitudes above 10 km. The tendency for increased errors at low altitude can be attributed to the large relative difference between the atmosphere-relative speed found in this work and in Withers and Murphy (2009).

5. Discussion

This work used the atmospheric entry of Opportunity as a case study to show that the concept of using Doppler-shifted direct-to-Earth transmissions to perform real-time trajectory and atmospheric structure reconstructions for entry probes is viable. The trajectory and atmospheric structure found for Opportunity in this work compare well with the results of analysis of accelerometer data from its atmospheric entry. Upcoming missions that might benefit from this technique include Mars Science Laboratory (2011 launch), ESA's Mars EDL technology demonstrator that will accompany the Mars Trace Gas Orbiter (2016 launch), subsequent Mars landers, and entry probes for Venus, Titan and the giant planets.

Although a detailed error analysis is not appropriate for this preliminary concept study, it is clear that many of the differences between the results of this work and those of Withers and Murphy (2009) can be attributed to the relatively crude data used here. If this technique were applied realistically, then knowledge of the transmitted frequency, times, and received frequencies would be significantly better than was possible for this work. Two steps are necessary before this technique can be relied upon to support future entry probes formally. First, it should be demonstrated using actual received frequencies, not values extracted from a published figure. Possible test cases include the Pioneer Venus probes (Counselman et al., 1980), Pathfinder (Wood et al., 1997), Spirit, Opportunity, Phoenix (Kornfeld et al., 2008), and the Galileo probe (Atkinson et al., 1998). Second, sensitivity studies and error analyses should be performed to quantify the expected accuracy of its results.

Acknowledgements

P.W. acknowledges Mike Bird and an anonymous reviewer, as well as fruitful discussions with many colleagues in the planetary entry probe and radio science communities.

References

Atkins, P.W., 2002. Physical Chemistry, sixth ed. W.H. Freeman,.

Atkinson, D.H., Pollack, J.B., Seiff, A., 1998. The Galileo probe Doppler wind experiment: measurement of the deep zonal winds on Jupiter. J. Geophys. Res. 103, 22911–22928.

Counselman, C.C., Gourevitch, S.A., King, R.W., Loriot, G.B., Ginsberg, E.S., 1980. Zonal and meridional circulation of the lower atmosphere of Venus determined by radio interferometry. J. Geophys. Res. 85, 8026–8030.

Desai, P.N., Knocke, P.C., 2004. Mars Exploration Rover entry, descent, and landing trajectory analysis. In: American Institute of Aeronautics and Astronautics paper 2004-5092, 42nd AIAA Aerospace Science Meeting in Reno, Nevada, USA.

Dzierma, Y., Bird, M.K., Dutta-Roy, R., Pérez-Ayúcar, M., Plettemeier, D., Edenhofer, P., 2007. Huygens probe descent dynamics inferred from channel B signal level measurements. Planet. Space Sci. 55 (November), 1886–1895.

Johnston, D., Asmar, S.W., Chang, C., Estabrook, P., Finely, S., Pham, T., Satorius, E., 2004. Radio science receiver support of the Mars Exploration Rover landings. In: Third ESA International Workshop on Tracking, Telemetry and Command Systems for Space Applications, Darmstadt, Germany, available online at ⟨http://hdl.handle.net/2014/39097⟩.

Karkoschka, E., Tomasko, M.G., Doose, L.R., See, C., McFarlane, E.A., Schröder, S.E., Rizk, B., 2007. DISR imaging and the geometry of the descent of the Huygens probe within Titan's atmosphere. Planet. Space Sci. 55, 1896–1935.

Kass, D.M., Schofield, J.T., Crisp, J., Bailey, E.S., Konefat, E.H., Lee, W.J., Litty, E.C., Manning, R.M., San Martin, A.M., Willis, R.J., Beebe, R.F., Murphy, J.R., Huber, L.F., 2004. PDS volume MERIMU_0001. In: MER1/MER2-M-IMU-4-EDL-V1.0, NASA Planetary Data System.

Kazeminejad, B., Atkinson, D.H., Pérez-Ayúcar, M., Lebreton, J., Sollazzo, C., 2007. Huygens' entry and descent through titan's atmosphere—methodology and results of the trajectory reconstruction. Planet. Space Sci. 55, 1845–1876.

Kornfeld, R.P., Garcia, M.D., Craig, L.E., Butman, S., Signori, G.M., 2008. Entry, descent, and landing communications for the 2007 Phoenix Mars lander. J. Spacecraft Rockets 45, 534–547.

Lodders, K., Fegley, B., 1998. The Planetary Scientist's Companion. Oxford University Press.

Lorenz, R.D., Zarnecki, J.C., Towner, M.C., Leese, M.R., Ball, A.J., Hathi, B., Hagermann, A., Ghafoor, N.A.L., 2007. Descent motions of the Huygens probe as measured by the surface science package (SSP): turbulent evidence for a cloud layer. Planet. Space Sci. 55, 1936–1948.

Magalhães, J.A., Schofield, J.T., Seiff, A., 1999. Results of the Mars Pathfinder atmospheric structure investigation. J. Geophys. Res. 104, 8943–8956.

Schoenenberger, M., Cheatwood, F.M., Desai, P.N., 2005. Static aerodynamics of the Mars Exploration Rover entry capsule. In: American Institute of Aeronautics and Astronautics paper 2005-0056, 43rd AIAA Aerospace Science Meeting in Reno, Nevada, USA.

Withers, P., Murphy, J.R., 2009. PDS volume MERIMU_0002. In: MER1/MER2-M-IMU-5-EDL-DERIVED-V1.0, NASA Planetary Data System.

Withers, P., Smith, M.D., 2006. Atmospheric entry profiles from the Mars Exploration Rovers spirit and opportunity. Icarus 185, 133–142.

Withers, P., Towner, M.C., Hathi, B., Zarnecki, J.C., 2003. Analysis of entry accelerometer data: a case study of Mars Pathfinder. Planet. Space Sci. 51, 541–561.

Wood, G.E., Asmar, S.W., Rebold, T.A., Lee, R.A., 1997. Mars Pathfinder entry, descent, and landing communications. JPL TDA Progress Report 42–131, available online at ⟨http://ipnpr.jpl.nasa.gov/progress_report/42-131/131I.pdf⟩.